Slow spin dynamics and self-sustained clusters in sparsely connected systems

Jacopo Rocchi[*] and David Saad[†]
Nonlinearity and Complexity Research Group, Aston University, Birmingham B4 7ET, United Kingdom

Chi Ho Yeung[‡]
Department of Science and Environmental Studies, The Education University of Hong Kong, Hong Kong

(Received 5 June 2017; revised manuscript received 30 April 2018; published 29 June 2018)

To identify emerging microscopic structures in low-temperature spin glasses, we study self-sustained clusters (SSC) in spin models defined on sparse random graphs. A message-passing algorithm is developed to determine the probability of individual spins to belong to SSC. We then compare the predicted SSC associations with the dynamical properties of spins obtained from numerical simulations and show that SSC association identifies individual slow-evolving spins. Studies of Erdos-Renyi (ER) and random regular (RR) graphs show that spins belonging to SSC are more stable with respect to spin-flip fluctuations, as suggested by the analysis of fully connected models. Further analyses show that SSC association outperforms local fields in predicting the spin dynamics, specifically the group of slow- and fast-evolving spins in RR graphs, for a wide temperature range close to the spin-glass transition. This insight gives rise to a powerful approach for predicting individual spin *dynamics* from a single snapshot of an equilibrium spin configuration, namely from limited *static* information. It also implies that single-sample SSC association carries more information than local fields in describing the state of individual spins, when little information can be extracted from the system's topology.

DOI: 10.1103/PhysRevE.97.062154

I. INTRODUCTION

Spin-glass models of disordered systems are characterized by a rich structure of the free-energy landscape and a nontrivial dynamics at low temperatures. Mean-field analyses [1–3] typically characterize the static properties of models based on a set of macroscopic order parameters [4,5], providing insight into their equilibrium properties and dynamical behavior [3,6].

Fully and sparsely connected models have been extensively studied using powerful tools such as the replica and cavity methods [4,7]. While the different temperature regimes are well understood in terms of the (free-) energy landscape, it is more difficult to describe their manifestation at the *microscopic* level. Interesting cases where this connection is clearer are constraint satisfaction problems studied at zero temperature, which give rise to solution clusters containing frozen variables in intermediate regimes prior to the satisfiability transition [8–13]. In addition to the insight gained, understanding the microscopic properties and their links to the system dynamics are essential for devising approximate optimization algorithms for specific instances.

Studies of the relation between system equilibrium properties and its dynamical behavior [14,15] show that it is possible to interpret system dynamical characteristics in terms of its ground-state structural properties. Moreover, they reveal interesting properties of the low-temperature dynamics such as the spontaneous timescale separation between slow and fast evolving spins. This phenomenon has been observed also in numerical experiments in systems defined on finite-dimensional lattices [16,17], giving rise to the notion of *rigidity lattice* [18]. Another approach linking equilibrium and dynamical properties [19], reveals that metastable states relate to fixed points of the generalized belief propagation (BP) in the two-dimensional (2D) Edwards-Anderson model. Similar problems have been studied in the context of glassy and jammed systems, where machine-learning algorithms have been used to identify local structures susceptible to local rearrangements [20].

Our approach aims to link equilibrium and dynamical properties of spin models on random graphs via the concept of *self-sustained clusters* (SSC) and the use of BP methods. The central objects of our approach are SSC, introduced in the study of the SK [21] and 3-spin Ising models [22]. By definition, the field induced by in-cluster spins, on spins belonging to an SSC, has a higher magnitude than the one induced by out-cluster spins. SSC can be regarded as metastable formations that correspond to suboptimal system configurations and explain the emergence of slow-evolving spins in fully connected models.

Here we focus on systems with simple discrete disorder ($J = \pm 1$) defined on Erdos-Renyi (ER) and random regular (RR) graphs. We develop and apply a BP algorithm to identify SSC variables in these settings and run dynamical simulations at different temperatures to study the relation between slow-evolving spins and SSC variables. More precisely, after equilibration for a long time, we sample a configuration and infer its SSC structure; this is then contrasted against its microscopic dynamics, starting from this configuration and monitoring the dynamical properties of individual spins, such

[*]j.rocchi@aston.ac.uk
[†]d.saad@aston.ac.uk
[‡]chyeung@eduhk.hk

as their flipping probability. We identify a strong relation between SSC association and slow-evolving spins for both ER and RR graphs, supporting the insight provided by our previous work [21] on densely connected models. We then compare the information contained in SSC membership variables to that of local fields on spin dynamics and find that SSC outperform local fields in identifying the slow- and fast-evolving spins for a wide temperature range around the spin-glass transition, especially in the RR case (due to the variable node connectivity of ER models the correlation is less emphasized). After defining the SSC framework of sparse graphs, we give details on the protocol employed for the simulations and analyze the obtained results.

II. FORMATION OF SELF-SUSTAINED CLUSTERS

Consider a pairwise Ising model on a sparse graph $\mathcal{G}$ with link weights $\{J_{ij}\}$ and a given spin configuration $\underline{s}$. In this paper, we study models with quenched coupling $J_{ij} = \pm 1$ with equal probabilities. We introduce an SSC membership variable σ_i equal to 1 when spin i belongs to an SSC and equal to 0 otherwise. This SSC condition is enforced by an indicator function,

$$\mathbb{I}(\underline{\sigma}|\underline{s},\mathcal{G}) = \prod_{i=1}^{N} \{(1-\sigma_i) + \sigma_i \theta[u_i^2 - v_i^2 - \epsilon]\}, \qquad (1)$$

taking the value of 1 if the set $\underline{\sigma} = \{\sigma_i\}_{i=1,\dots,N}$ identifies a SSC and zero otherwise, where u_i and v_i are the in-cluster and out-cluster induced fields, respectively, defined by

$$u_i = \sum_{m\in\partial i} J_{im}\sigma_m s_m \quad \text{and} \quad v_i = \sum_{m\in\partial i} J_{im}(1-\sigma_m)s_m, \qquad (2)$$

where ∂i denotes the set of neighbors of node i. The sum of the two fields constitutes the total field

$$h_i = \sum_{m\in\partial i} J_{im}s_m = u_i + v_i. \qquad (3)$$

The resilience parameter ϵ is defined by the condition $u_i^2 > v_i^2 + \epsilon$ and indicates the strength of the cluster. The set of all the possible $\underline{\sigma}$ vectors that satisfy Eq. (1) corresponds to all the possible SSC structures given the spin configuration $\underline{s}$. It is important to notice that the trivial realizations $\sigma_i = 0\ \forall i$ and $\sigma_i = 1\ \forall i$ satisfy Eq. (1): They correspond to the cases where there are no SSC or when the only SSC is the complete system, respectively.

III. BELIEF PROPAGATION EQUATIONS

The variable σ_i depends on the state of the variables $\sigma_{j\in\partial i}$ defined on all the neighbors of node i. It is convenient to define a factor graph, but a conventional factor graph gives rise to many short loops that hamper convergence and proper calculation of the marginals. As in similar cases [23], we will introduce a superfactor graph of supervariables $S_{ij} = (\sigma_{ij},\sigma_{ji})$ comprising the states of variable pairs $\sigma_{ij} = \sigma_i$ and $\sigma_{ji} = \sigma_j$. The variable σ_i is copied in all the supervariables associated with node i, as shown in Fig. 1, while the different indices j in σ_{ij} refer to neighboring links. We consider the double-index variables as independent states but enforce their equality

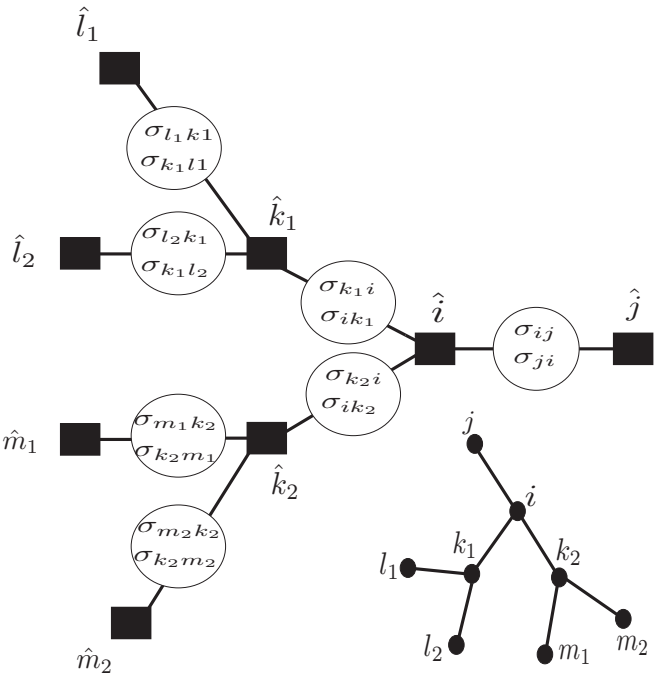

FIG. 1. A superfactor graph corresponding to the original graph at the bottom right of the figure. Each supervariable contains two variables of the original graph. For each node of the original graph $\mathcal{G}$ we have a superfactor and for each link we have a supervariable. All the variables $\sigma_{ik}, \forall k \in \partial i$ are forced to be the same by the superfactors' constraint. The superfactor and original graphs share the same topology.

through the superfactors,

$$\psi_{\hat{i}}^{S}(\underline{S}_{\partial\hat{i}}) = \psi_{\hat{i}}(\underline{\sigma}_{\partial\hat{i}}) \prod_{k\in\partial i} \delta_{\sigma_{ik},\sigma_i} \qquad (4)$$

defined on the original node i and denoted by $\hat{i}$ in the superfactor graph, where $\psi_{\hat{i}}(\underline{\sigma}_{\partial\hat{i}})$ is given by

$$\psi_{\hat{i}}(\underline{\sigma}_{\partial\hat{i}}) = \{(1-\sigma_i) + \sigma_i\theta[u_i^2 - v_i^2 - \epsilon]\}. \qquad (5)$$

More details are provided in the Appendix.

The BP equations for this supergraph read

$$\nu_{\hat{i}\to(ij)}(S_{ij}) \propto \sum_{S_{ki}\in\underline{S}_{\partial\hat{i}}\setminus S_{ij}} \psi_{\hat{i}}^{S}(\underline{S}_{\partial\hat{i}}) \prod_{k\in\partial i\setminus j} \eta_{(ki)\to\hat{i}}(S_{ki}), \qquad (6)$$

where, given the pairwise nature of the interactions in the original graph, messages from the supervariables to the superfactors take the form

$$\eta_{(ij)\to\hat{j}}(S_{ij}) \propto \nu_{\hat{i}\to(ij)}(S_{ij}). \qquad (7)$$

These equations can be simplified in a single line to

$$m_{i\to j}(\sigma_i,\sigma_j) \propto \sum_{\underline{\sigma}_{\partial i\setminus j}} \psi_{\hat{i}}(\underline{\sigma}_{\partial\hat{i}}) \prod_{k\in\partial i\setminus j} m_{k\to i}(\sigma_k,\sigma_i), \qquad (8)$$

where we define the messages $m_{i\to j}(\sigma_i,\sigma_j) = \eta_{(ij)\to\hat{j}}(S_{ij}) = \nu_{\hat{i}\to(ij)}(S_{ij})$. Marginals of the supervariables can be computed from the equation

$$\eta_{(ij)}(S_{ij}) \propto \nu_{\hat{i}\to(ij)}(S_{ij})\nu_{\hat{j}\to(ij)}(S_{ji}) \qquad (9)$$

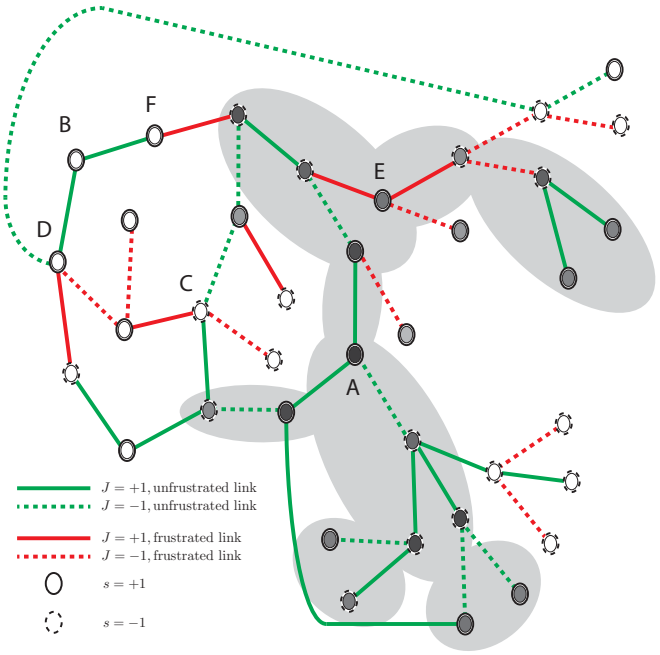

FIG. 2. A toy model which comprises 38 spin variables. Unfrustrated links are marked in green and frustrated links in red. Positive J and s are denoted by solid lines and circles, respectively, while negatives J and s are denoted by dashed lines and circles, respectively. White nodes represents $p(\sigma_i=1)=0$ and black $p(\sigma_i=1)=1$; the gray region identifies nodes for which $p(\sigma_i)>0.5$.

and can be used to compute single-node marginals

$$p(\sigma_i)=\sum_{\sigma_j}\eta_{(ij)}(S_{ij})=\sum_{\sigma_j}m_{i\to j}(\sigma_i,\sigma_j)m_{j\to i}(\sigma_j,\sigma_i). \quad (10)$$

Single-node marginals have to satisfy a consistency check since $p(\sigma_i)$ could be computed from $\sum_{\sigma_k}\eta_{(ik)}(S_{ik})$ for all nodes $k\in\partial i$. Thus, after convergence, this condition is checked to assess the quality of the obtained marginals.

IV. TOY MODEL

To illustrate how the BP method identifies SSC nodes, we constructed a toy model comprising 38 spins as shown in Fig. 2. In this case a specific configuration $\underline{s}$ is considered and the corresponding SSC memberships marginals $p(\sigma_i),\forall i$, are calculated. Node colors represent the value of $p(\sigma_i)$ in a gray scale; white represents $p(\sigma_i=1)=0$ and black $p(\sigma_i=1)=1$. The gray *region* identifies nodes for which $p(\sigma_i)>0.5$.

We observe that spins which do not experience frustration (green edges or variables) are more likely to belong to an SSC, but this is true only if their neighbors are also part of the SSC. For instance, while both nodes A and B do not experience frustration $p(\sigma_A)=0.91$ while $p(\sigma_B)=0$. It is instructive to investigate why the neighbors of B are not part of the SSC: nodes D and F receive conflicting messages from their neighbors and thus the local fields acting on them are 0; hence they cannot be part of an SSC and, consequently, node B is not part of an SSC either. The situation of node C is similar to that of node D. Interestingly, we observe that node E *is* part of the SSC. This is counterintuitive because in the sampled spin configuration this node is frustrated, having all the links unsatisfied. However, since two of its neighbors are part of the SSC and the three links can be satisfied by a single spin flip, node E is identified as being within an SSC, having a probability $p(\sigma_E)=0.66$. The last consideration is also clearly related to the notion of dynamical timescale separation; following a single flip, spin E experiences the same large absolute value of the local field with all of its links satisfied. Spins that belong to regions with smaller degree of frustration are less likely to flip, at least singularly. The dynamics is local and such spins are already close to a configuration that minimizes the energy in the local region. The evidence that the SSC association is robust enough to recognize such nontrivial spin associations suggests that it may be used to effectively identify slow evolving variables in spin-glass dynamics, as we argue in the next sections.

V. RESULTS

We consider spin-glass models of $N=1000$ spins defined on ER and RR topologies and implement a sequential Glauber dynamics in the spin-glass phase starting from a random configuration. For (mean) connectivity equal to c, the critical inverse temperatures for the spin-glass transition are known for both models [24] to be

$$\beta_c^{\mathrm{ER}}=\operatorname{arctanh}\left(\frac{1}{\sqrt{c}}\right),\quad \beta_c^{\mathrm{RR}}=\operatorname{arctanh}\left(\frac{1}{\sqrt{c-1}}\right). \quad (11)$$

To carry out our experiments we first equilibrate the system and then monitor the flipping dynamics. This is implemented in two stages:

(i) *From initial conditions to equilibrium:* We implement Glauber dynamics at an inverse-temperature β_1 and wait for t_1 dynamical sweeps, where one *sweep* is defined by updating the whole system, we sample a single configuration (the significance of t_1 is explained later). In this configuration we study the SSC structure by running the BP algorithm with $\epsilon=0.1$, which allows us to associate each spin with the corresponding SSC-membership probability $p_i^+=p(\sigma_i=1)$.

(ii) *Flipping dynamics*: We then conduct the following experiment: Starting from the sampled configuration from stage one, we study at least 200 trajectories of the system at different inverse temperatures β_2 for t_2 sweeps; for each temperature we consider the number of flips per spin. We readily obtain the flip rates ρ_i of spin i by dividing the number of its spin-flips at stage two by t_2. If the self-sustained structure contains information about the system dynamics, flip rates ρ and SSC marginal probabilities p^+ should be anticorrelated, and a scatter plot of these two quantities for all variables should demonstrate this behavior.

To quantitatively measure the relation between SSC association and flip rate, we rank spins according to their p^+ values by defining a rank r_j such that $r_1=\operatorname{argmin}_i(p_i^+)$ and $r_N=\operatorname{argmax}_i(p_i^+)$. We further define a normalized rank $\tilde{r}=r/N$, and a function of cumulative flip rate as

$$f(\tilde{r})=\frac{1}{Z}\sum_{j=1}^{N}\rho_{r_j}\Theta(\tilde{r}-\tilde{r}_j), \quad (12)$$

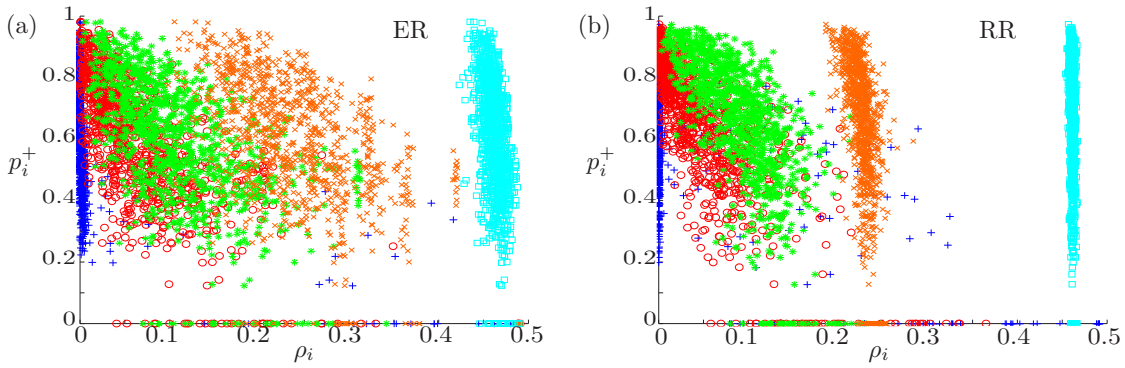

FIG. 3. Scatter plot of p_i^+ and ρ_i for dynamics on (a) a Erdos-Renyi graph of mean connectivity $c = 6$ and (b) a random regular graph of connectivity $c = 6$. A configuration is sampled at $\beta_1 = 5$ after $t_1 = 10^4$ sweeps. As discussed in the text, from this configuration we ran 1000 simulations that we observed for $t_2 = 100$ Monte Carlo Sweeps (MCS), which can been used to compute ρ_i. The symbols {+, o, ∗ , x, and □} refer to dynamics at $\beta_2 = 3, 1, 0.7, 0.4,$ and 0.1, respectively. Spin-glass transition inverse temperatures are $\beta_6^{\mathrm{ER}} \sim 0.387$ and $\beta_6^{\mathrm{RR}} \sim 0.420$.

where Z is the normalization constant $Z = \sum_i^N \rho_i$ and $\Theta(\tilde{r} - \tilde{r}_j)$ is the step function, returning one for a positive argument and zero otherwise. The function $f(\tilde{r})$ is thus similar to the receiver operating characteristics (ROC) curve, when the SSC association is considered as a predictor for slow dynamics, and provides the fraction of total flips explained by the low p^+ variables. For instance, one can see that the gradient of $f(\tilde{r})$ is proportional to the flip rate of spin with rank equal to $\tilde{r}$ [i.e., $f'(\tilde{r}) \propto \rho_{r_j}$ for $\tilde{r}_j \leqslant \tilde{r} < \tilde{r}_{j+1}$], implying that the steeper the slope of $f(\tilde{r})$, the faster the flip rate of spins ranked at $\tilde{r}$. If $f(\tilde{r})$ is steeper for small $\tilde{r}$ than for large $\tilde{r}$, ranked by the SSC probabilities, then spins with small SSC probabilities tend to flip faster. In this case, the area under the ROC curve (AUC) $f(\tilde{r})$ quantifies the information contained in the SSC marginal probabilities about the future flip rate or the negative coorelation between them. The values of AUC are bounded between $0 \leqslant \mathrm{AUC} \leqslant 1$. The absence of information yields an AUC value of 0.5, and the more negative the correlation between SSC probabilities and future flip rates, the larger the AUC value.

A. Dependence on flipping temperatures β_2

Figure 3 show a scatter plot of p_i^+ and ρ_i for ER and RR topologies of (mean) connectivity 6, respectively, where in both cases p_i^+ are computed on the configuration sampled after $t_1 = 10^4$ sweeps at $\beta_1 = 5$ in stage one, and ρ_i is measured for dynamics starting from this configuration at $\beta_2 = 3, 1, 0.7, 0.4, 0.1$ in stage two. While for large β_2 there is a strong relation between spins with high SSC membership marginals p_i^+ and small flip rate ρ_i, this relation disappears as β_2 decreases. Furthermore, as shown in the insets of Figs. 4(a) and 4(b), the ROC curve at $\beta_2 = 0.1$ almost diagonal, implying that there is no statistical dependence between p_i^+ and ρ_i in this case. Nevertheless, the ROC curves separate from the diagonal line and point to a meaningful predictive power of the p_i^+ ranking as β_2 increases, implying a stronger tendency for spins with small (large) SSC probabilities p_i^+ to flip faster (slower). To quantify this connection we compute the values of AUC under the ROC curves. As shown in Figs. 4(a) and 4(b), AUC increases from a value of 0.5 at small β_2 to a value close to 1 as β_2 increases, implying a change from zero correlation

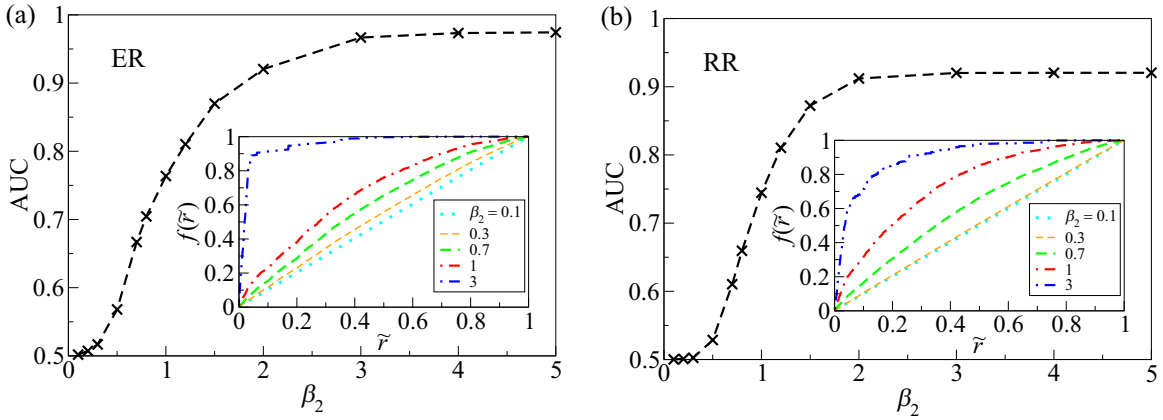

FIG. 4. The AUC values for the ROC curves defined by Eq. (12), of cumulative flip rate by ranking spins according to their SSC marginal probabilities, obtained for (a) Erdos-Renyi graphs and (b) random regular graphs with $N = 1000$ vertices and degree connectivity $c = 6$, as a function of flipping inverse temperature β_2, with waiting time $t_1 = 10^4$, sampling inverse temperature $\beta_1 = 5$, and flipping time $t_2 = 100$ over 200 trajectories. Each data point is averaged over 10 realizations of graph topologies. Inset: The ROC curves at different β_2 on (a) Erdos-Renyi graphs and (b) random regular graphs. The closer the sampling temperature β_2 is to the configuration temperature β_1 the more accurate is the SSC association is as a predictor of slow spin dynamics.

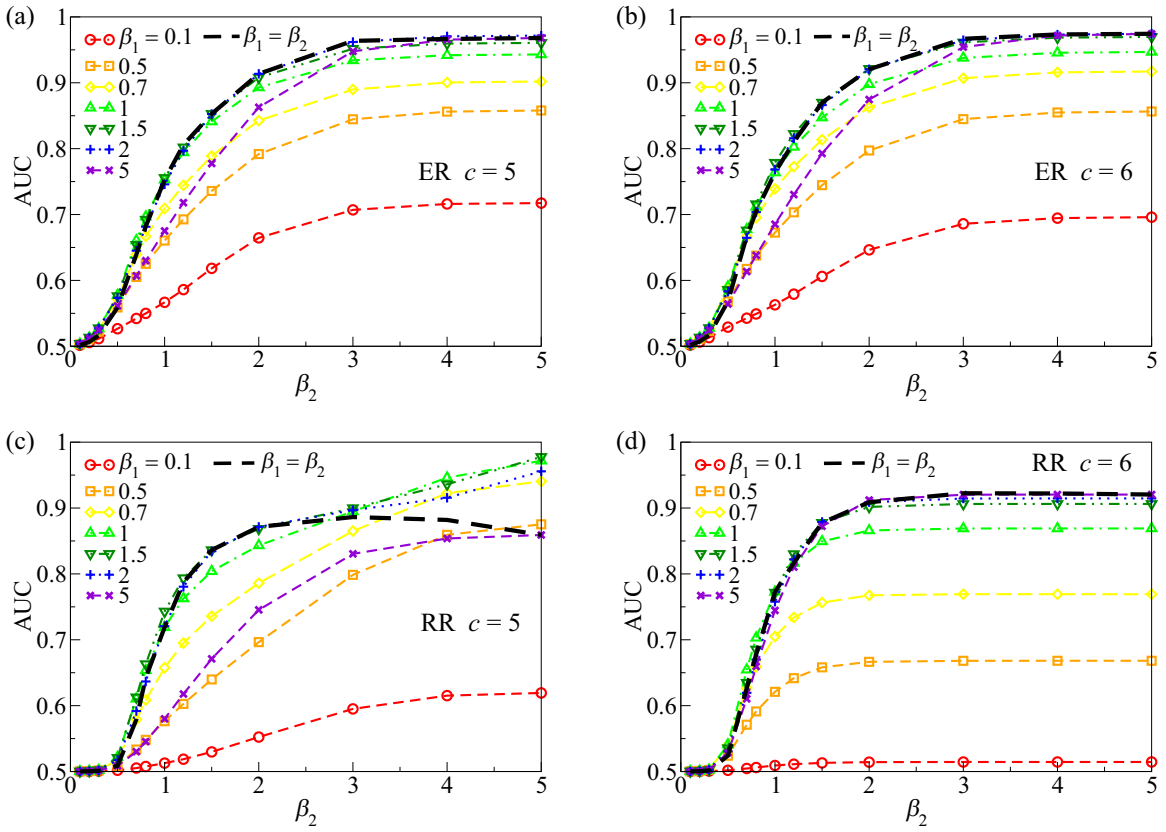

FIG. 5. The AUC obtained on ER graphs with (a) $c = 5$ and (b) $c = 6$, and RR graphs with (c) $c = 5$ and (d) $c = 6$, with $N = 1000$, waiting time $t_1 = 10^4$, and flipping time $t_2 = 100$, at different sampling temperatures β_1 as a function of flipping temperatures β_2 over 200 trajectories. Each data point is averaged over 10 realizations of graph topologies.

between p_i^+ and ρ_i at a large temperatures (small β_2) to a strong correlation at a low temperatures (large β_2).

These results can be interpreted as follows: the SSC structure of the configurations sampled at very low temperatures after a long waiting time describes a metastable arrangement of spins with long-range correlations. At low temperatures in stage two the SSC spins remain close to the sampled configuration of stage one, especially for SSC-associated spins with $p_i^+ \sim 1$, which flip less frequently than those with smaller p_i^+ values. The inverse spin-glass transition temperatures in these two cases are $\beta^{\rm ER} \sim 0.387$ and $\beta^{\rm RR} \sim 0.420$, which are roughly the values of β_2 that show the onset of an abrupt increase in AUC from AUC $= 0.5$ as shown in Figs. 4(a) and 4(b). This also explains why the relation between p_i^+ and ρ_i can be observed in a larger range of temperatures compared to the RR case in the ER case shown in Fig. 3(a): While $\beta_2 = 0.4$ is in the spin-glass phase for the ER model, it is not so for the RR model. We also notice in Fig. 3 that for both cases the sampled configuration includes spins with $p_i^+ = 0$. Interestingly, these spins flip more frequently at high β_2 (for instance, $\beta_2 = 3,5$) where the dynamics exhibit many slow variables and a few fast evolving ones: A possible explanation for this is that, at high β_2, spins with fields close to zero flip with a very high probability as soon as their field crosses from positive to negative value and vice versa; additionally, close-to-zero fields will be more common at high β_2 since many spins are highly aligned with bipolar values, and an even number of strongly aligned contributions would balance the field value of those spins with $p_i^+ = 0$. At lower β_2 this behavior is mitigated by the lower flip probability at field values close to zero as well as by the broader distribution of field values as many spins are less-strongly aligned. In general, these results show that spins with a higher SSC probability tend to be dynamically more stable and vice versa. It further implies that SSC can be used as a tool to predict individual spin dynamics based on a single snapshot of equilibrium spin configuration.

B. Dependence on sampling temperatures β_1

To examine the relation between SSC probabilities and flip rates we plot in Figs. 5(a)–5(d) the AUC values at different sampling temperatures β_1 and flipping temperatures β_2 for the cases of odd and even degrees in ER and RR graphs. Except for the case of RR graphs with $c = 5$ of Fig. 5(c), all other cases show a similar behavior: The AUC increases with decreasing flipping temperatures (i.e., increasing β_2) at all sampling temperatures β_1; the AUC also increases with lower sampling temperatures (i.e., higher β_1). It implies that the power of SSC probabilities is most significant at both low sampling and flipping temperatures for the cases of Figs. 5(a), 5(b) and 5(d). This can be explained by the fact that at a very low flipping temperature such as $\beta_2 = 5$, SSC sampled in stage one are stable for a long time. Thus, spins identified to be in SSC tend to flip fewer times in stage two, unless the SSC is destabilized.

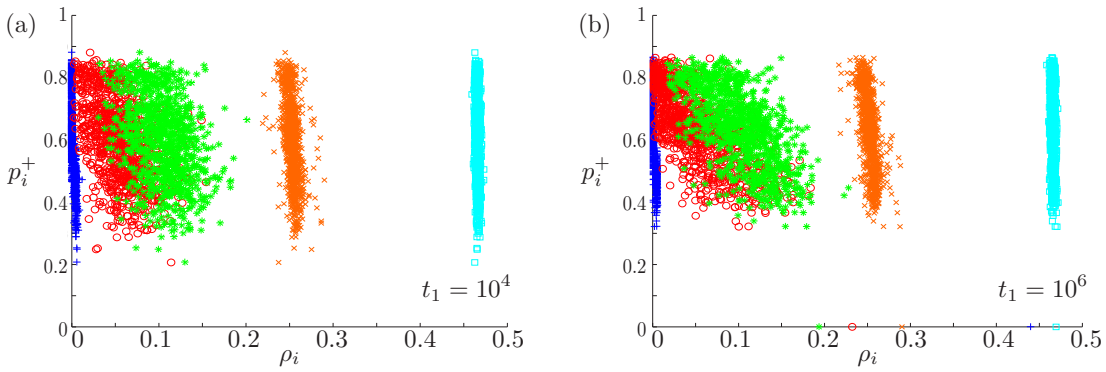

FIG. 6. Scatter plot of p_i^+ and ρ_i for dynamics on an RR graph of connectivity equal to 5. A configuration is sampled at $\beta_1 = 5$ after (a) $t_1 = 10^4$ sweeps and (b) $t_1 = 10^6$ sweeps. As discussed in the text, from this configuration we ran 1000 simulations that we observed for 100 MCS, which can been used to compute ρ_i. The symbols {+, o, ∗, x, and □} refer to dynamics at $\beta_2 = 3, 1, 0.7, 0.4$, and 0.1, respectively. Inverse spin-glass temperature in this case is $\beta_{c=5}^{\mathrm{RR}} \sim 0.464$.

However, we note that a low sampling temperature (high β_1) in stage one does not necessarily lead to the highest identifying power at all flipping temperatures in stage two. For instance, as shown in Figs. 5(a) and 5(b) of ER graphs, the values of AUC with $\beta_1 = 5$ are lower than that with $\beta_1 = 1$ or 1.5 for an intermediate range of flipping temperatures with β_2 around 1. In a way, this is not surprising since the probabilities for SSC association are sampled at a given temperature and are therefore most relevant for predicting the dynamics at that temperature. We note that SSC sampled at $\beta_1 = 1$ or 1.5 are in the glassy phase but close to the transition temperatures, making them more relevant for that temperature range than to SSC that are sampled at a much lower temperature (e.g., $\beta_1 = 5$). Similar behaviors are observed for RR graphs with $c = 6$ in Fig. 5(d). These results show that low-temperature SSC do not always have the strongest predictive power across the whole range of flipping temperatures at stage two, particularly when at very low temperatures the dynamics is frozen on the timescales t_2 analyzed here.

Hence, one may expect that cases with a matching pair of sampling and flipping temperatures, i.e., $\beta_1 = \beta_2$, lead to the highest AUC at all β_2. The results for this case are shown in Figs. 5(a), 5(b) and 5(d) denoted by thick dashed lines without a symbol. As we can see, these AUC values are close to the highest attained values at all β_2, but they are not exactly the highest for the cases with small $\beta_2 \sim 0.1$ to 1. This is expected since SSC sampled at a high temperature (i.e., small $\beta_1 = \beta_2$) are easily destabilized by thermal fluctuations, and hence they have a small predictive power for the flip rate. On the other hand, SSC sampled at intermediate temperatures with $\beta_1 = 1$ or 1.5, which are below but close to the phase transition temperatures, identify very successfully structures of slow evolving variables in the high-temperature regime.

Finally, we discuss the case of $c = 5$ for RR graphs shown in Fig. 5(c). As we can see, the results are generally consistent with the other cases of Figs. 5(a), 5(b) and 5(d), where AUC values increase with decreasing β_1 and β_2, except that at a very low sampling temperatures (e.g., large $\beta_1 = 2$ or 5), AUC values *decrease* with β_2. This behavior may be related to recent findings in the closely related minimal defensive alliance problem [25] in RR graphs with uniform couplings, where small alliances are more difficult to identify by lowering the temperature in the case with $c = 5$ than for $c = 6$. These may lead to the degradation in predictive power of SSC dynamics sampled at very low temperatures.

C. Dependence on waiting time t_1 and flipping time t_2

To further examine the identifying power of SSC marginal probabilities, we study the effect of different waiting times t_1 in stage one for the same flipping times t_2 in stage two. Figures 6(a) and 6(b) show the scatter plots of p_i^+ vs. ρ_i for two waiting times $t_1 = 10^4$ and $t_1 = 10^6$ sweeps for RR topologies of connectivity $c = 5$, the correlated behavior described above is more emphasized when longer waiting times are used; i.e., data points (of p_i^+ vs. ρ_i) at low temperatures have steeper and more well-defined slopes in the case $t_1 = 10^6$. The AUC values corresponding to Figs. 6(a) and 6(b) are shown in Fig. 7 as the lines with cross and square symbols, where AUC values in the cases with $t_1 = 10^6$ are substantially higher than those with $t_1 = 10^4$. In general, the longer the waiting time t_1, the higher the AUC for all flipping temperatures β_2 as shown in

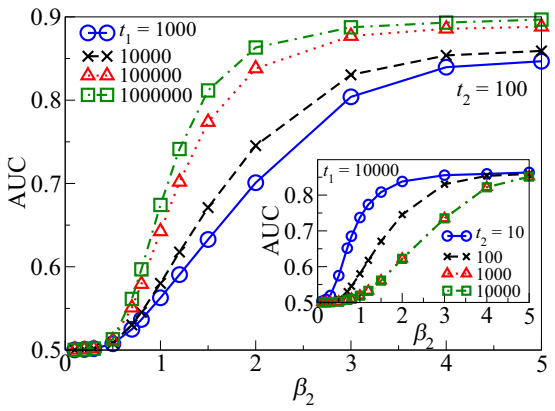

FIG. 7. The AUC values obtained for random regular graphs with $N = 1000$ and $c = 5$, with $\beta_1 = 5$ and different waiting times t_1 in stage one, but the same flipping time $t_2 = 100$ in stage two. Inset: The AUC values with the same waiting time $t_1 = 10\,000$ in stage one but a different t_2 in stage two.

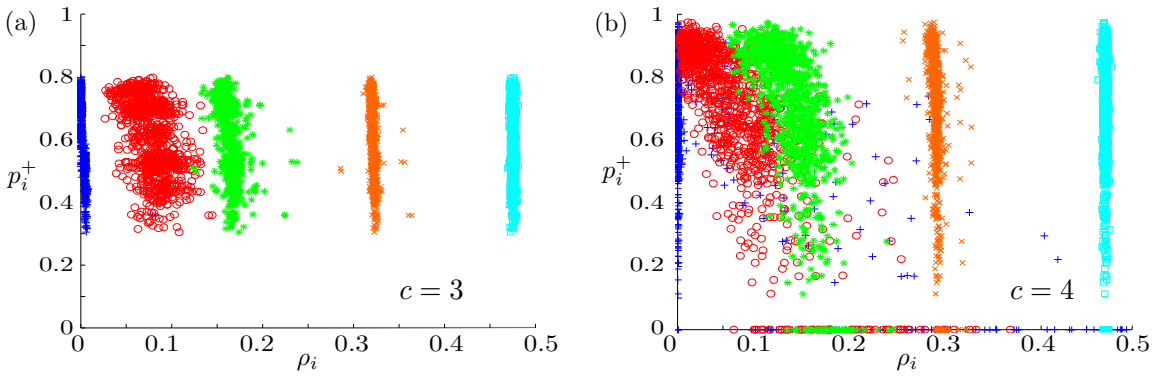

FIG. 8. Scatter plot of p_i^+ and ρ_i for the dynamics on an RR graph of connectivities (a) $c = 3$ and (b) $c = 4$. A configuration is sampled at $\beta_1 = 5$ after $t_1 = 10^4$ sweeps. As discussed in the text, from this configuration we ran 1000 simulations that we observed for $t_2 = 100$ MCS, which can been used to compute ρ_i. The symbols {+, o, ∗, x, and □} refer to dynamics at $\beta_2 = 3, 1, 0.7, 0.4$, and 0.1, respectively. Spin-glass transition inverse temperatures are $\beta_{c=3}^{\mathrm{RR}} \sim 0.615$ and $\beta_{c=4}^{\mathrm{RR}} \sim 0.524$.

Fig. 7. This implies that the snapshots of SSC structures taken after a long time are more stable and more representative of the equilibrium configurations and hence can identify stable spins with a greater accuracy.

We also notice that the timescale separation between fast and slow spins at low temperatures disappears in the case of $c = 5$ shown in Figs. 6(a) and 6(b) compared to the case of $c = 6$ in Fig. 3(b). Consistently, our algorithm does not find spins where $p_i^+ = 0$ in the case with $c = 5$. In order to investigate this effect further, we extended the analysis to RR topologies of different connectivities, studying the cases of $c = 3,4$. We find that timescale separation at low temperatures appears only for even connectives in RR graphs. We attribute this behavior to the strong residual field in odd degree connections in comparison to the even case, were close-to-zero fields may exist due to balanced contribution from neighboring spins. To support this conjecture we consider RR graphs of connectivities $c = 3,4$, observing the expected behavior as shown in Fig. 8. In the first case $c = 3$ we do not find very large or very small values of p_i^+ and, consistently, the timescale separation emerging for even degree connectives is much weaker. On the other hand, in the second case $c = 4$ the results resemble those of Fig. 3.

We then examine the dependence of the results on the flipping times t_2 in stage two given the same equilibration time t_1 in stage one. As we can see from the inset of Fig. 7, the longer the flipping time, the smaller the AUC values. This is an expected behavior as the longer the time we measure the flip rate, the more likely the SSC in the sampled configurations, of spins with large p^+ values, become destabilized. In summary, the identifying power of SSC is stronger given a longer waiting time t_1 and a shorter flipping time t_2.

D. Dynamics on Erdös-Rényi graphs

In the case of ER graphs, the dynamics at $\beta \sim \beta^{\mathrm{ER}}$ exhibits a broader range of flipping frequencies. This effect is not visible in the RR case and is due to its degree heterogeneity as can be observed in Figs. 9 and 10. We also observe that the dependence on t_1 discussed in Fig. 6 for the RR case is not as evident in the ER case.

E. Comparison of identifying power of SSC and local fields

Finally, to benchmark the forecasting power of SSC, we compare the prediction by the SSC marginal probabilities p_i^+

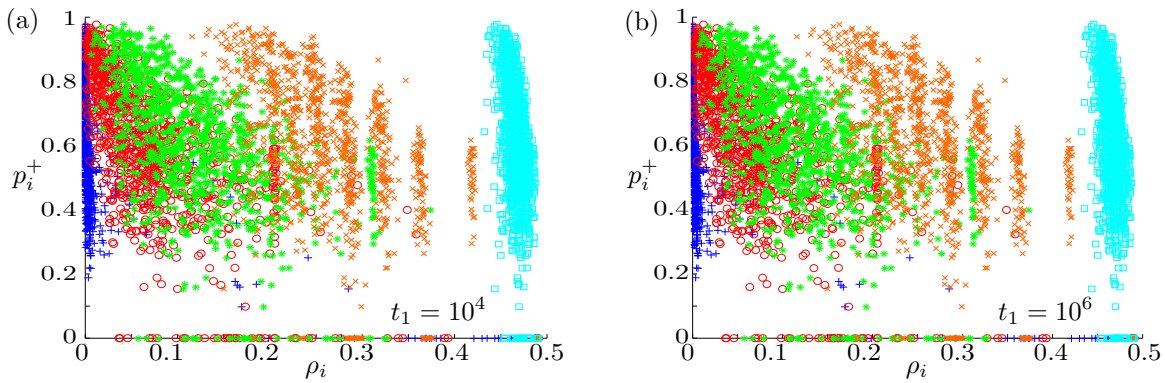

FIG. 9. Scatter plot of p_i^+ and ρ_i for the dynamics on an ER graph of mean connectivity 5. A configuration is sampled at $\beta_1 = 5$ after (a) $t_1 = 10^4$ sweeps and (b) $t_1 = 10^6$ sweeps. From this configuration we ran 1000 simulations that we observed for $t_2 = 100$ MCS to compute ρ_i. The symbols {+, o, ∗, x, and □} refer to dynamics at $\beta_2 = 3, 1, 0.7, 0.4$, and 0.1, respectively. Inverse spin-glass temperature in this case is $\beta_{c=5}^{\mathrm{ER}} \sim 0.420$.

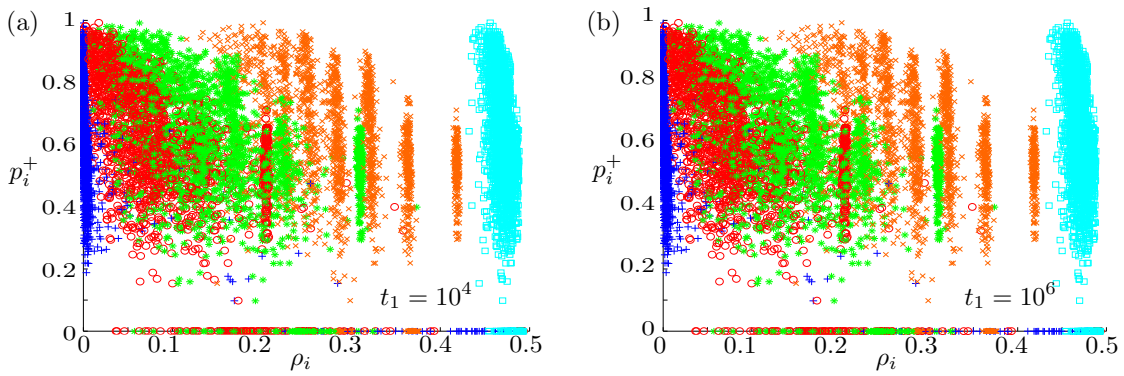

FIG. 10. Scatter plot of p_i^+ and ρ_i for the dynamics on an ER graph of mean connectivity equal to 3. A configuration is sampled at $\beta_1 = 5$ after (a) $t_1 = 10^4$ sweeps and (b) $t_1 = 10^6$ sweeps. From this configuration we ran 1000 simulations that we observed for $t_2 = 100$ MCS to compute ρ_i. The symbols {+, o, ∗, x, and □} refer to dynamics at $\beta_2 = 3, 1, 0.7, 0.4,$ and 0.1, respectively. Inverse spin-glass temperature in this case is $\beta_{c=3}^{\mathrm{ER}} \sim 0.523$.

with that of the local field $h_i = \sum_{k\in\partial i} J_{ij} s_j$. In the sampled configuration at stage one, we compute the local fields of each individual spin and expect that the higher the local field of a spin is the slower its flip rate would be at stage two. In this case, similarly to p_i^+, one can rank spins in ascending order of local field magnitude and use Eq. (12) to obtain an AUC value which characterizes the identifying power of local fields for the future flip rate.

We show the fractional difference of the two predictions in Fig. 11(a) in four different cases of RR and ER graphs with even- and odd-degree connectivities. As we can see, the differences are mostly positive in the RR case, meaning that SSC outperform local fields in predicting the flip rate of spins but not so in the ER case. Moreover, we observe an underperformance of the SSC-association predictor on ER graphs with small β_2 and RR graphs with with large β_2. The reason for this may be due to the fact that h_i is correlated with the degree c_i in ER graphs. As a result, connectivity and thus local fields in ER graphs, are already good predictors of flip rate at high temperatures. The underperformance by SSC in RR graphs with $c = 5$ may be due to the decrease in AUC values with β_2 as shown by the dashed line with $\beta_1 = \beta_2$ in Fig. 5(a). On the other hand, we note that SSC outperforms local fields by almost 20% at $\beta_2 = 0.5$ in both cases with $c = 5$ and $c = 6$, roughly the corresponding transition temperatures in RR graphs. This may imply that SSC has the strongest identifying power over local fields in the cases when the systems are close to the phase transition in the RR graphs.

In the inset of Fig. 11(a), we show the AUC values of flip rate obtained by SSC probabilities p_i^+ and local fields in the case of RR graphs with $c = 6$. As we can see, the AUC values obtained by SSC are higher than that obtained by the local fields for most values of flipping temperature β_2, which means that SSC has a stronger identifying power than local fields in this case.

To further understand the identifying power of SSC, we analyze the flip-rate distribution. Since flip rate is continuous, we bin the flip rate into 100 equally distributed bins in the range between 0 and 1 and compute the flip-rate distribution $Q(\rho)$ over all spins, $Q_{\mathrm{slow}}(\rho)$, over spins with the top 20% of p_i^+ or $|h_i|$ values (presumably slow spins), and $Q_{\mathrm{fast}}(\rho)$ over spins with the bottom 20% of p_i^+ or $|h_i|$ values. We compute the Kullback-Leibler (KL) divergence between $Q(\rho)$ with $Q_{\mathrm{slow}}(\rho)$ as

$$D_{\mathrm{slow}} = -\sum_j Q_j^{\mathrm{slow}} \log \frac{Q_j^{\mathrm{slow}}}{Q_j}, \tag{13}$$

where j is the bin index. Similarly, we can define the KL divergence D_{fast} for fast spins. The larger the KL divergence, the larger the difference between Q_{slow} or Q_{fast} is from the overall spin distributions Q and the more different is the behavior of the identified group of slow or fast spins from the whole group, which points to a stronger identifying power of the predictors.

As we can see in the inset of Fig. 11(b), the D_{slow} measure for the SSC predictor is larger than that obtained for local fields in the case of RR with $c = 6$, meaning that SSC have a stronger identifying power than local fields in identifying slow spins. The fractional difference of D_{slow} by the two predictors is plotted in Fig. 11(b), showing that the SSC-based predictor outperforms local fields one in identifying slow spins in RR graphs with both $c = 5$ and $c = 6$ for the examined range of flipping temperatures β_2. Interestingly, the highest outperformance is found near $\beta_2 \approx 0.5$, similarly to those observed for AUC in Fig. 11(a) and close to the transition temperatures. On the other hand, for ER graphs, the values of D_{slow} predicted by SSC and local fields are similar.

Finally, we examine the identifying power of fast spins by the two predictors. As shown in Fig. 11(c) and the inset, the SSC-based predictor outperforms the local fields-based one in the case of RR with both $c = 5$ and $c = 6$, similarly to the results in terms of AUC and D_{slow}. It implies that even when the connectivity in the graph is uniform, SSC can still provide a good prediction for slow and fast spins compared to the prediction by local fields. In other words, by only considering a snapshot of the system, SSC marginal probabilities carry more information about the state of an individual spin than its local field. For ER graphs, the SSC-based predictor outperforms local fields one for large β_2 but underperform at intermediate β_2. It may implies that SSC are not good at identifying fast spins in ER graphs as fast spins are mostly nodes of small degrees experiencing small field magnitudes. As a result, local field magnitude may already be a good predictor for fast spins in ER graphs.

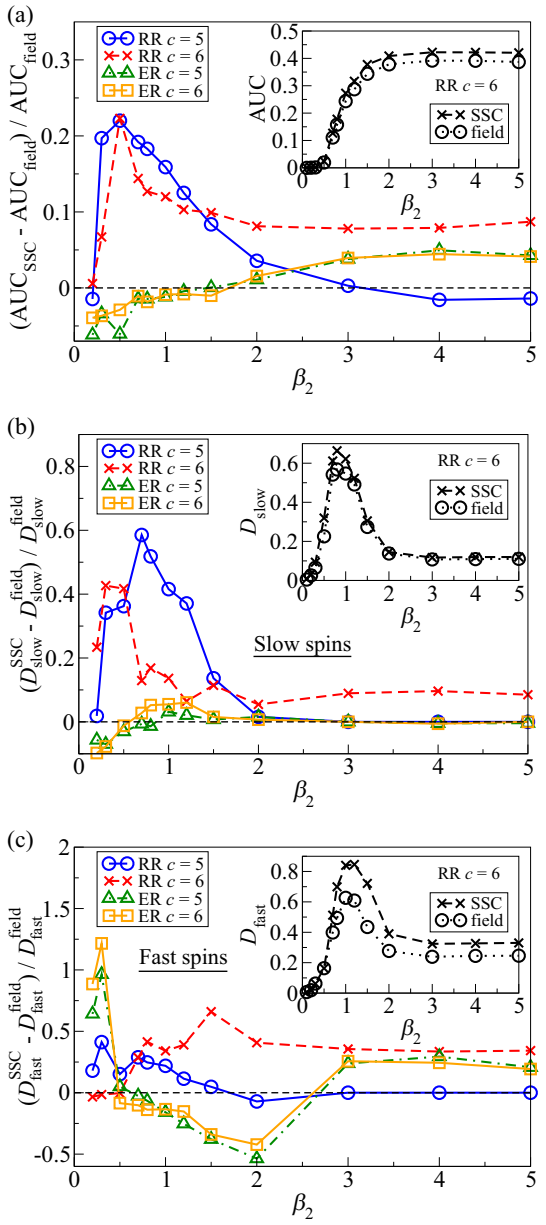

FIG. 11. Comparing the difference in values of (a) AUC, (b) KL divergence D_{slow} between the flip-rate distributions of slow spins (i.e., large-p^+ or large-field spins) and all spins, and (c) KL divergence D_{fast} between the flip-rate distributions of fast spins (i.e., small-p^+ or small-field spins) and all spins, obtained by the SSC-based prediction and local fields. The results are obtained for $t_1 = 10\,000$, $t_2 = 100$ on graphs with $N = 1000$, and by setting $\beta_1 = \beta_2$. The data at $\beta_2 = 0.1$ are omitted since the AUC values D_{slow} and D_{fast} are very small in this case and result in large fluctuations in the fractional difference. Insets: The AUC and the two KL divergences D_{slow} and D_{fast} values in the case of RR graphs with $N = 1000$ and $c = 6$.

We showed that given a snapshot of the system at equilibrium, SSC provide a powerful predictor for the dynamical properties of individual spins, especially in uniform connectivity profiles. As the rationale of SSC can be extended to systems in other areas, these results suggest that the same methodology can be used to devise generic tools for identifying the dynamical properties of variables in a wide range of applications based on limited static information.

VI. SUMMARY

We developed a theoretical framework linking dynamical and equilibrium properties of spin-glass models on sparse graphs based on the concept of SSC, which can be viewed as regions of interdependent mutually stabilizing spins. We show that the SSC structure of a given sampled configuration predicts the dynamical properties of the system, such as the microscopic timescale separation in certain systems and regions of slow-evolving variables in spin systems. This supports the conjecture made in our previous work where we studied analytically the properties of SSC in fully connected models. We show that the marginal probabilities for a spin to be associated with an SSC has a stronger identifying power than its local field magnitude in identifying its subsequent flip rate; our results suggest that SSC-based indicators may be especially useful in the case of RR graphs close to their transition point. We provide a new microscopic perspective on the low-temperature dynamics of spin-glass systems with the potential of developing new algorithmic optimization tools for hard computational problems through the destabilization of SSC. Furthermore, our results show that the SSC paradigm can be used as a tool to predict individual spin dynamics based on a single snapshot of equilibrium spin configuration, which can be extended to applications in other areas.

ACKNOWLEDGMENTS

This work is supported by The Leverhulme Trust (Grant No. RPG-2013-48), and grants from the Research Grants Council of the Hong Kong Special Administrative Region, China (Project No. EdUHK ECS 28300215, GRF 18304316, and GRF 18301217). We thank F. Ricci-Tersenghi for interesting discussions.

APPENDIX

Factor graphs and belief propagation equations

This section explains the need for a superfactor graph of supernodes that comprise variable pairs due to the emergence

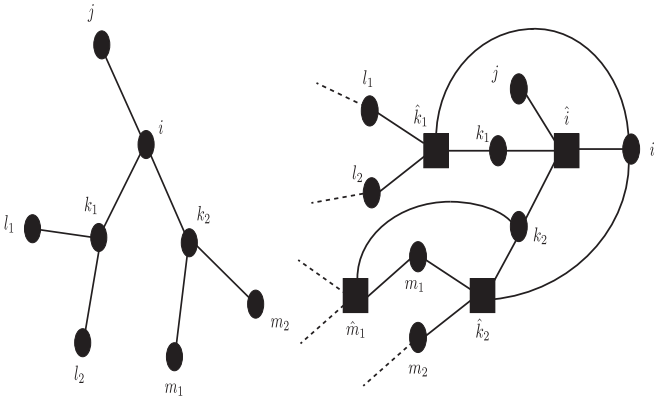

FIG. 12. The original graph topology (left) specified by the tree $\mathcal{G}$ and corresponding factor graph for the SSC problem (right), which clearly include many small loops.

of many loops if a single-variable factor graph is introduced. Let us consider the graph on left side of Fig. 12. In this graph, we would like to compute the marginals for σ's values. To this aim, we introduce the factor graph on the right side of Fig. 12. Typically, the message factor $\hat{i}$ sends to node i can be written as

$$\nu_{\hat{i}\to i}(\sigma_i) \propto \sum_{\underline{\sigma}_{\partial\hat{i}\setminus i}} \psi_{\hat{i}}(\underline{\sigma}_{\partial\hat{i}}) \prod_{k\in\partial\hat{i}\setminus i} \eta_{k\to\hat{i}}(\sigma_k), \tag{A1}$$

while the message node k sends to factor $\hat{i}$ becomes

$$\eta_{k\to\hat{i}}(\sigma_k) \propto \prod_{\hat{k}\in\partial k\setminus i} \nu_{\hat{k}\to k}(\sigma_k). \tag{A2}$$

This is a standard procedure to compute marginals on treelike topologies; the interested reader can find more details in Ref. [26]. This factor graph contains small loops due to the dependence of variables on the neighbors of their neighbors. In other words, the state of variable σ_i depends on the state of all of its neighbors, whose state depend on σ_i itself. This is a notorious problem for implementing BP and inferring the related marginals. To overcome this problem we introduce a modified factor graph with supervariables formed by variable pairs as explained in the main text, see Fig. 1, where there are no small loops, since its structure is the same as that of the original graph. We can also observe that this supergraph can be created by considering a superfactor for each node, and a supervariable for each link of the original graph.

[1] D. Sherrington and S. Kirkpatrick, Phys. Rev. Lett. **35**, 1792 (1975).
[2] G. Parisi, Phys. Rev. Lett. **43**, 1754 (1979).
[3] J.-P. Bouchaud, L. F. Cugliandolo, J. Kurchan, and M. Mezard, in *Spin Glasses and Random Fields* (World Scientific, Singapore, 1998), Vol. 12, pp. 161–223.
[4] M. Mézard, G. Parisi, and M.-A. Virasoro, in *Spin Glass Theory and Beyond* (World Scientific, Singapore, 1990).
[5] G Parisi, in *Complex Systems*, edited by J.-P. Bouchaud, M. Mézard, and J. Dalibard (Elsevier, Les Houches, France, 2007).
[6] E. Marinari, G. Parisi, F. Ricci-Tersenghi, J. J. Ruiz-Lorenzo, and F. Zuliani, J. Stat. Phys. **98**, 973 (2000).
[7] M. Mézard and G. Parisi, Eur. Phys. J. B **20**, 217 (2001).
[8] M. Mézard, F. Ricci-Tersenghi, and R. Zecchina, J. Stat. Phys. **111**, 505 (2003).
[9] F. Krzakała, A. Montanari, F. Ricci-Tersenghi, G. Semerjian, and L. Zdeborová, Proc. Natl. Acad. Sci. USA **104**, 10318 (2007).
[10] A. Montanari, F. Ricci-Tersenghi, and G. Semerjian, J. Stat. Mech. (2008) P04004.
[11] D. Achlioptas and F. Ricci-Tersenghi, SIAM J. Comput. **39**, 260 (2009).
[12] G. Semerjian, J. Stat. Phys. **130**, 251 (2008).
[13] A. Braunstein, L. Dall'Asta, G. Semerjian, and L. Zdeborová, J. Stat. Mech. (2016) 053401.
[14] A. Barrat and R. Zecchina, Phys. Rev. E **59**, 1299(R) (1999).
[15] F. Ricci-Tersenghi and R. Zecchina, Phys. Rev. E **62**, R7567 (2000).
[16] F. Romá, S. Bustingorry, and P. M. Gleiser, Phys. Rev. Lett. **96**, 167205 (2006).
[17] F. Romá, S. Bustingorry, and P. M. Gleiser, Phys. Rev. B **81**, 104412 (2010).
[18] F. Barahona, R. Maynard, R. Rammal, and J. P. Uhry, J. Phys. A: Math. Gen. **15**, 673 (1982).
[19] A Lage-Castellanos, R. Mulet, and F. Ricci-Tersenghi, Europhys. Lett. **107**, 57011 (2014).
[20] E. D. Cubuk, S. S. Schoenholz, J. M. Rieser, B. D. Malone, J. Rottler, D. J. Durian, E. Kaxiras, and A. J. Liu, Phys. Rev. Lett. **114**, 108001 (2015).
[21] C.-H. Yeung and D. Saad, Phys. Rev. E **88**, 032132 (2013).
[22] J. Rocchi, D. Saad, and C.-H. Yeung, Phys. Rev. B **96**, 024415 (2017).
[23] K. Y. M. Wong and D. Saad, J. Phys. A **41**, 324023 (2008).
[24] D. J. Thouless, Phys. Rev. Lett. **56**, 1082 (1986).
[25] Y.-Z. Xu, C. H. Yeung, H.-J. Zhou, and D. Saad, arXiv:1802.04047.
[26] M. Mezard and A. Montanari, *Information, Physics, and Computation* (Oxford University Press, New York, 2009).